VISCOPLASTIC SEISMIC RESPONSE OF ARCH DAM UNDER HIGH HYDROSTATIC PRESSURE

S.Y. Xiao[1] and G. Lin[2]

[1] *Associate Professor, The Key State Laboratory of Coastal and Offshore, Dalian University of technology, Dalian. China*

[2] *Professor, The Key State Laboratory of Coastal and Offshore, Dalian University of technology, Dalian. China*
Email: shyxiao@dlut.edu.cn, gaolin@dlut.edu.cn

ABSTRACT :
In this paper, seismic responses of a 278m high arch dam were analyzed. The consistency viscoplastic Hsieh-Ting-Chen four-parameter model of concrete, modified from the static Hsieh-Ting-Chen four-parameter model based on the results of uniaxial tensile and compressive dynamic tests of concrete, was adopted. This model took account into the effect of strain rates and hydrostatic pressure on dynamic behaviors of concrete. Then, an implicit backward Euler iterative algorithm was proposed. Results showed that the strain rate affected the first principal stresses, the maximal equivalent visco-plastic strain rate of the arch dam. It played an important role in the safety assessment of arch dams located in earthquake active area.
KEYWORDS: arch dam, seismic response, strain rate, hydrostatic pressure, constitutive model, algorithm

1. INTRODUCTION

Many high arch dams have been built and will be built in high seismic area in China. Some of them will reach 300 meters in height. For researchers and engineers, the greatest concern was the safety of these structures against earthquake shocks. During the past two or three decades, many sophisticated computer programs have been developed and used for numerical analysis of the arch dams. Our ability to analyze mathematical models of dam structures subjected to earthquake ground motions has improved dramatically. Nevertheless, the current design practice in the seismic design of arch dams was still based on the linear elastic assumption. The key property which determines the capacity of arch dams to withstand earthquakes was the tensile strength of concrete. However, the design criterion for the tensile stress was still a problem at issue. A widely accepted standard was not available. The conventional design practice accounts for rate sensitivity by means of drastic simplifying assumptions. That was, in all cases, the allowable stresses of an arch dam under earthquake load were increased by, such as a Chinese Standard (2001), 30% of the value specified for static case. Similarly, the dynamic modulus of elasticity was assigned 30% higher than its static value.
Concrete is a typical rate-dependent material: its strength, stiffness and ductility (or brittleness) are affected by loading rates. Research on the rate dependency of concrete started in 1917 with Abrams' dynamic compressive experiment. Based on the experimental results, Norris (1959) proposed an empirical formula and predicted that the compressive strengths should increase up to 33%, 24% and 17% greater than the static strength when the strain rates were $3s^{-1}$, $0.3s^{-1}$ and $0.1s^{-1}$, respectively. Bischoff (1991) reviewed and analyzed the dynamic compressive experiments of concrete and deduced that the confusion about the increased magnitude of dynamic strengths arose because many factors, such as concrete quality, aggregate, age, curing, and moisture conditions, had influenced the behavior during rapid loading. The reported dynamic tensile tests of concrete in literature were more difficult to perform. Zielinski (1981) studied the behaviors of concrete subjected to uniaxial impact tensile loading and found that the ratios of impact and static tensile strengths were between 1.33 and 2.34 for various concrete mixes. Tedesco (1991) conducted the direct tension tests of plain concrete specimens on a split-Hopkinson pressure bar to investigate the effects of increasing strain rate on the tensile strength of concrete. Rossi (1994) made an experimental study of rate effects on the behaviors of concrete under tensile stress to investigate the effect of the water/cement ratio on the tensile strength enhancement. In addition, an analysis of the physical mechanisms was developed to investigate how the Stefan effect, the cracking process, and the inertia forces participated together in the dynamic behavior of a specimen subjected to a uniaxial tensile test (Rossi, 1996). Malvar (1998) reviewed the extant data characterizing the effects of strain rate on the tensile strength of concrete and compared the DIF (dynamic increase factor) formulation with that recommended by the European CEB. Finally, an alternative formulation was proposed based on the experimental data.
As for the concrete of dams, Rapheal (1984) carried out the dynamic test of concrete from dam cores and

reported an average dynamic-static splitting tensile strength ratio of 1.45, and an average dynamic-static compressive strength ratio of 1.31 for the same loading rate ranges. Harris (2000) performed the laboratory tests on concrete cores drilled from dams and tested at strain rates that simulated dynamic and static loading conditions. Results indicated that dynamic-static strength ratios were greater than these for both the tensile and compressive strength tests.

Few researchers considered the effect of strain rates on dynamic responses of arch dams because there was lack of the rate-dependent dynamic constitutive models of concrete. Cervera (1996) developed a rate-dependent isotropic damage model for the numerical analysis of concrete dams. The application of the proposed model to the seismic analysis of a large gravity concrete dam showed that the tensile peak strength of concrete could be increased up to 50 percent for the range of strain rates that appear in a structural safety analysis of a dam subjected to severe seismic actions. Lee (1998) developed a plastic-damage model for concrete subjected to cyclic loading using concepts of fracture-energy-based damage and stiffness degradation. The rate-dependent regularization was used to guarantee a unique converged solution for softening regions. No effect for rate-dependency on the stress distribution was involved. Chen (2004) proposed a rate-dependent damage constitutive model for massive concrete by introducing rate-dependant plastic damage variables as internal variables. The nonlinear seismic responses of arch dams were computed using this model and the results were compared with the results given by the corresponding rate-independent damage model. It was shown that the distribution of strain rates not only influenced the vibration modes of dam, but also had significant effects on the dynamic damage of arch dams. Bai (2006) established a rate-dependent damage constitutive model for simulating the mechanical behaviors of concrete by introducing the effect of strain rates into the damage tensor. The model was applied to analyze the seismic overload response of a typical concrete gravity dam. Results indicated that the distribution of strain rates caused by seismic loading varied at the dam surface and significantly affected the dynamic response.

2.MODEL AND PARAMETERS OF ARCH DAM

In order to illustrate the effect of the rate dependency on the dynamic structural response, a 278m high arch dam in China subjected to earthquake excitation was analyzed by the proposed model. The dam and the foundation were discretized into 450 and 1040 three-dimensional isoparametric 8-node elements respectively. **Fig.1** showed the discretized dam-foundation system.

The material properties for the study were as follows: for the dam body, the elastic module was 2.4×10^4MPa, the Poisson's ratio was 0.17, the density was 2.4×10^3kg/m^3, static compressive strength was 30MPa, and static tensile strength was 2.5MPa; for the foundation rock, the elastic module was 1.6×10^4MPa, the Poisson's ratio was 0.25, the density was 2.0×10^3kg/m^3. The high of water level was 540m. The five lowest vibration frequencies of the dam: f_1 =1.332Hz, f_2 =1.406Hz, f_3 =1.544Hz, f_4 =1.631Hz and f_5 =1.689Hz. An assumption of massless foundation was introduced to simplifying the dam-foundation interaction analysis though more rigorous interaction effects can be included.

Three-dimensional earthquake waves were used as the input. The design horizontal earthquake acceleration was 0.321 gal and the vertical acceleration was 0.214 gal. **Fig.2** showed the typical artificial unitary acceleragram that met the requirement of Chinese Specifications for Seismic Design of Hydraulic Structures.

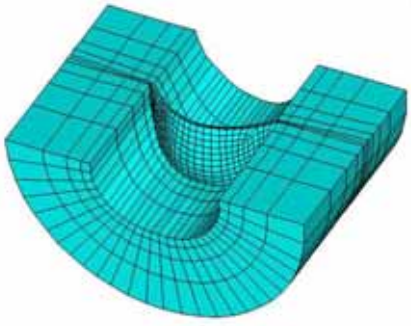

Fig.1 Geometry and mesh of arch dam

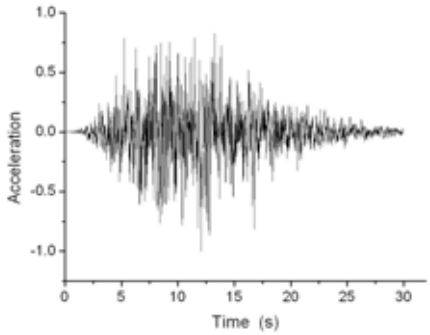

Fig.2 Time history of earthquake input

3.RATE-DEPENDENT CONSTITUTIVE MODEL OF CONCRETE

3.1. Consistency viscoplastic model theory

The consistency viscoelastic model could be seen as an extension of the classic elastic-plastic model to account for the rate-dependent behavior of materials. This model, which used the Von Mises yield surface, had been applied by Wang (1997) to analyze metal. With this method, the consistency viscoelastic Hoffman model of concrete was modified by Winnicki (2001). In this model, during viscoplastic flow, the actual stress state must remain on the yield surface and the consistency condition was imposed.

The viscoplastic yield function could be expressed as

$$F(\sigma_{ij},\kappa,\dot{\kappa})=0 \quad \text{for} \quad \dot{\lambda}>0 \tag{3.1}$$

In uniaxial compression and tension, equation (3.1) could be expressed as

$$F_c=F(\sigma_{ij},\kappa_c,\dot{\kappa}_c) \qquad F_t=F(\sigma_{ij},\kappa_t,\dot{\kappa}_t) \tag{3.2}$$

It was difficult to establish biaxial or triaxial constitution relationships because of the lack of biaxial or triaxial dynamic experiment results of concrete. Generally, biaxial compressive strength of concrete was considered as an increase to the uniaxial compressive strength such that

$$f_{bc}=K_{bc}f_c=K_{bc}f(\sigma_{ij},\kappa_c,\dot{\kappa}_c) \tag{3.3}$$

On an arbitrary stress state, it was assumed that

$$\kappa_c=\varphi_c(\sigma_{ij})\kappa \qquad \kappa_t=\varphi_t(\sigma_{ij})\kappa \tag{3.4}$$

Where, $\varphi_c(\sigma_{ij})$ and $\varphi_t(\sigma_{ij})$ were the weight functions of the invariable.

Using such conditions, the yield function could be expressed as

$$F(\sigma_{ij},\kappa,\dot{\kappa})=F(\sigma_{ij},\kappa_c,\dot{\kappa}_c,\kappa_t,\dot{\kappa}_t)=0 \tag{3.5}$$

At the same time, the viscoplastic consistency condition must be satisfied so that

$$\frac{\partial F}{\partial\sigma_{ij}}d\sigma_{ij}+\frac{\partial F}{\partial\kappa_c}d\kappa_c+\frac{\partial F}{\partial\dot{\kappa}_c}d\dot{\kappa}_c+\frac{\partial F}{\partial\kappa_t}d\kappa_t+\frac{\partial F}{\partial\dot{\kappa}_t}d\dot{\kappa}_t=0 \tag{3.6}$$

The effects of κ_t and $\dot{\kappa}_t$ on f_t were assumed to be independent and the instantaneous tensile strength f_t was formulated in a very general way as

$$f_t=f_{ts}H_t(\kappa_t)R_t(\dot{\kappa}_t) \tag{3.7}$$

Similarly, the instantaneous compressive strength was computed as

$$f_c=f_{cs}H_c(\kappa_c)R_c(\dot{\kappa}_c) \tag{3.8}$$

where $H_t(\kappa_t)$, $R_t(\dot{\kappa}_t)$ and $H_c(\kappa_c)$ and $R_c(\dot{\kappa}_c)$ were assumption functions achieved by experiment. In this paper, κ was adopted as $\kappa=\bar{\varepsilon}^{VP}=\sqrt{2\varepsilon_{ij}^{vp}\varepsilon_{ij}^{vp}/3}$.

3.2. Consistency viscoplastic Hsieh-Ting-Chen four-parameter model of concrete

In this study, the yield surface function was assumed to be the same as the failure surface function of concrete, so the yield function of the HTC (Hsieh-Ting-Chen) four-parameter model could be expressed as

$$F(I_1,J_2,\theta)=aJ_2+(d\cos\theta+c)\sqrt{J_2}+bI_1-1=0 \tag{3.9}$$

where four parameters a, b, c and d were chosen by four conditions：1) uniaxial tensile strength f_t, 2) uniaxial compressive strength f_c, and 3) biaxial compressive strength $f_{bc}=k_{bc}f_c$, and 4) the stress state at the compressive meridian $(\sigma_{oct},\tau_{oct})=(-k_1f_c,k_2f_c)$.

Defining $m_{ij}=\dfrac{\partial F}{\partial\sigma_{ij}}$ and according to the classic HTC four-parameter model, the relationship between θ and σ_{ij} was given as follows:

$$\cos 3\theta = \frac{3\sqrt{3}}{2} \cdot \frac{J_3}{J_2^{3/2}} \tag{3.10}$$

So,

$$\begin{aligned} m_{ij} &= \frac{\partial F}{\partial I_1} \cdot \frac{\partial I_1}{\partial \sigma_{ij}} + \frac{\partial F}{\partial J_2}\frac{\partial J_2}{\partial \sigma_{ij}} + \frac{\partial F}{\partial \theta}\left(\frac{\partial \theta}{\partial J_2}\frac{\partial J_2}{\partial \sigma_{ij}} + \frac{\partial \theta}{\partial J_3}\frac{\partial J_3}{\partial \sigma_{ij}}\right) \\ &= \alpha\delta_{ij} + \beta s_{ij} + \gamma t_{ij} \end{aligned} \tag{3.11}$$

where $\delta_{ij} = \partial I_1 / \partial \sigma_{ij}$, $s_{ij} = \partial J_2 / \partial \sigma_{ij}$, $t_{ij} = \dfrac{\partial J_3}{\partial \sigma_{ij}}$.

In equation (3.6), $\dfrac{\partial F}{\partial \kappa_c}$, $\dfrac{\partial F}{\partial \dot{\kappa}_c}$, $\dfrac{\partial F}{\partial \kappa_t}$ and $\dfrac{\partial F}{\partial \dot{\kappa}_t}$ could be achieved by uniaxial compressive and tensile tests of concrete.

Based on the associated plastic flow rule, viscoplastic strain was defined as

$$d\varepsilon_{ij}^{vp} = d\lambda \frac{\partial F}{\partial \sigma_{ij}} = d\lambda m_{ij} \tag{3.12}$$

The invariable could be expressed as

$$d\kappa = \sqrt{\frac{2}{3} d\varepsilon_{ij}^{vp} d\varepsilon_{ij}^{vp}} = \sqrt{\frac{2}{3} m_{ij} m_{ij}}\, d\lambda = g(\sigma_{ij}) d\lambda \tag{3.13}$$

Using these functions, the consistency equation (3.6) could be expressed as

$$m_{ij} d\sigma_{ij} + h d\lambda + s d\dot{\lambda} = 0 \tag{3.14}$$

where

$$h = \frac{\partial F}{\partial \lambda} = \frac{\partial F}{\partial f_c} f_{cs} \varphi_c(\sigma_{ij}) g(\sigma_{ij}) \frac{\partial H_c(\kappa_c)}{\partial \kappa_c} R_c(\dot{\kappa}_c) + \frac{\partial F}{\partial f_t} f_{ts} \varphi_t(\sigma_{ij}) g(\sigma_{ij}) \frac{\partial H_t(\kappa_t)}{\partial \kappa_t} R_t(\dot{\kappa}_t)$$

$$s = \frac{\partial F}{\partial \dot{\lambda}} = \frac{\partial F}{\partial f_c} f_{cs} \varphi_c(\sigma_{ij}) g(\sigma_{ij}) H_c(\kappa_c) \frac{\partial R_c(\dot{\kappa}_c)}{\partial \dot{\kappa}_c} + \frac{\partial F}{\partial f_t} f_{ts} \varphi_t(\sigma_{ij}) g(\sigma_{ij}) H_t(\kappa_t) \frac{\partial R_t(\dot{\kappa}_t)}{\partial \dot{\kappa}_t}$$

Dynamic tensile and compressive tests of were carried out to investigate the effect of strain rates on the dynamic tensile and compressive behaviors of concrete (Xiao, 2008). Test results indicate that the tensile and compressive strengths of concrete increased with the loading rate. The initial tangential modulus and the critical strain of concrete in tension were independent of strain rate but those in compression slightly increased with the strain rate. Poisson's ratio of concrete in both tension and compression was not obviously dependent on loading rate.

3.3. Euler return mapping algorithm

At the time t, the stress σ_{ij}^t, the invariable κ^t and the rate of invariable $\dot{\kappa}^t$ should satisfy the yield condition,

$$F(\sigma_{ij}^t, \kappa^t, \dot{\kappa}^t) = 0 \tag{3.15}$$

At the time $t + \Delta t$, the stress could be written as

$$\sigma_{ij}^{t+\Delta t} = \sigma_{ij}^t + \Delta\sigma_{ij} = \sigma_{ij}^t + D_{ijkl}^{ep}(\sigma_{ij}, \Delta\lambda)\Delta\varepsilon_{kl} \tag{3.16}$$

where $D_{ijkl}^{ep}(\sigma_{ij}, \Delta\lambda)$ was the tangent module of the consistency viscoplastic model.

Also, the stress $\sigma_{ij}^{t+\Delta t}$, the invariable $\kappa^{t+\Delta t}$ and the rate of invariable $\dot{\kappa}^{t+\Delta t}$ at the time $t + \Delta t$ should satisfy the yield condition. At the short time increment, the assumption was an approximation for $\dot{\lambda}$ as

$$\dot{\lambda} = \frac{\lambda^{t+\Delta t}}{\Delta t} \tag{3.17}$$

Therefore, the internal parameter $\kappa^{t+\Delta t}$ and its rate $\dot{\kappa}^{t+\Delta t}$ could be written as

$$\dot{\kappa}^{t+\Delta t} = \dot{\lambda}^{t+\Delta t} g(\sigma_{ij}^{t+\Delta t}) = \frac{\Delta\lambda^{t+\Delta t}}{\Delta t} g(\sigma_{ij}^{t+\Delta t}) \tag{3.18}$$

$$\kappa^{t+\Delta t} = \kappa^{t} + \Delta\lambda^{t+\Delta t} g(\sigma_{ij}^{t+\Delta t}) \tag{3.19}$$

Consequently, using the above expression, the yield condition at the time $t+\Delta t$ could be formulated as in the classic rate-independent plasticity as follow:

$$F(\sigma_{ij}^{t+\Delta t}, \Delta\lambda^{t+\Delta t}) = 0 \tag{3.20}$$

During the k th iteration at the time $t+\Delta t$, the stress σ_{ij}^{k} and plastic multiplier $\Delta\lambda^{k}$ might not satisfy the yield condition

$$F^{k}(\sigma_{ij}^{k}, \Delta\lambda^{k}) \neq 0 \tag{3.21}$$

Generally, the stress σ_{ij}^{k} was not the real stress $\sigma_{ij}^{t+\Delta t}$ at the end of the given time $t+\Delta t$. So, the residual stress could be expressed as

$$r_{ij}^{k}(\sigma_{ij}^{k}, \Delta\lambda^{k}) = \sigma_{ij}^{k} - \sigma_{ij}^{t+\Delta t} = \sigma_{ij}^{k} - \sigma_{ij}^{t} - D_{ijkl}^{ep}(\sigma_{ij}, \Delta\lambda)\Delta\varepsilon_{kl} \tag{3.22}$$

During the $(k+1)$ th iteration at the time $t+\Delta t$, the yield function value F^{k+1} and the residual stress r_{ij}^{k+1} cloud be achieved from the truncated Taylor's series expansion of the yield F and the residual stress r_{ij} about position k, and then set to zero

$$F^{k+1} = F^{k} + \frac{\partial F^{k}}{\partial \sigma_{ij}}\delta\sigma_{ij}^{k} + \frac{\partial F^{k}}{\partial \Delta\lambda}\delta\Delta\lambda^{k} = 0 \tag{3.23}$$

$$r_{ij}^{k+1} = r_{ij}^{k} + \frac{\partial r^{k}}{\partial \sigma_{ij}}\delta\sigma_{ij}^{k} + \frac{\partial r^{k}}{\partial \Delta\lambda}\delta\Delta\lambda^{k} = 0 \tag{3.24}$$

Equations (3.23) and (3.24) represented a set of linear equations for the iterative stress update $\delta\sigma_{ij}^{k}$ and the iterative viscoplastic multiplier update $\delta\Delta\lambda^{k}$.
Defining

$$[\mathbf{A}] = \begin{bmatrix} \dfrac{\partial F^{k}}{\partial \Delta\lambda} & \dfrac{\partial F^{k}}{\partial \sigma_{ij}} \\ \dfrac{\partial r^{k}}{\partial \Delta\lambda} & \dfrac{\partial r^{k}}{\partial \sigma_{ij}} \end{bmatrix} \qquad \{\mathbf{b}\} = \begin{Bmatrix} -F^{k} \\ -r_{ij}^{k} \end{Bmatrix}$$

Equations (3.23) and (3.24) could be expressed as

$$[\boldsymbol{A}]\begin{Bmatrix} \delta\Delta\lambda^{k} \\ \delta\sigma_{ij}^{k} \end{Bmatrix} = \{\boldsymbol{b}\} \tag{3.25}$$

Taking into account the symmetry of the stress tensor, the iterative stress update $\delta\sigma_{ij}^{k}$ and the iterative viscoplastic multiplier update $\delta\Delta\lambda^{k}$ could be achieved by solving the set of linear equations. The iteration process continued until the norms $|F|$ and $|r_{ij}|$ became reasonably small. The final values of $\Delta\lambda$ and $\Delta\sigma_{ij}$ at the end of the time step were obtained by a summation process:

$$\Delta\lambda = \sum_{k=1}^{N} \delta\Delta\lambda^{k} \tag{3.26}$$

$$\Delta\sigma_{ij} = \sum_{k=1}^{N} \delta\sigma_{ij}^{k} \tag{3.27}$$

where N was the total number of iterations.

4.Seismic response of arch dam

4.1. stress of arch dam

The dynamic response analyses of the arch dam were performed at three models: model I (linear elastic model), model II (rate-independent Hsieh-Ting-Chen four-parameter model) and model III (rate-dependent Hsieh-Ting-Chen four-parameter model). The maximum values of the first and the third principle stress in the dam were shown in the Table1.

Table1 Maximal principal stress of arch dam

model	The first principal stress MPa	The third principal stress MPa
model I	5.10	-10.13
model II	2.96	-10.13
model III	3.14	-10.13

Fig.3 showed the distribution of the third principle stress obtained from three models. It was seen that in all three cases, the maximum compressive stress values were the same and they appeared at the bottom of the upstream face, the material remained working in the elastic range. However, for the maximum tensile stress there was marked difference among the calculated results of three models. Owing to the plasticity of concrete, the maximal values of the first principal stress of model II and III decreased 41.96% and 38.43% than model I, respectively. Because the dynamic tensile strength of concrete increased with strain rates, the maximal values of the first principal stress of model III, taken account into the effect of strain rates, increased 6.08% than model II. Fig.4, Fig.5 and Fig.6 showed the distribution of the first principle stress obtained from three models, respectively.

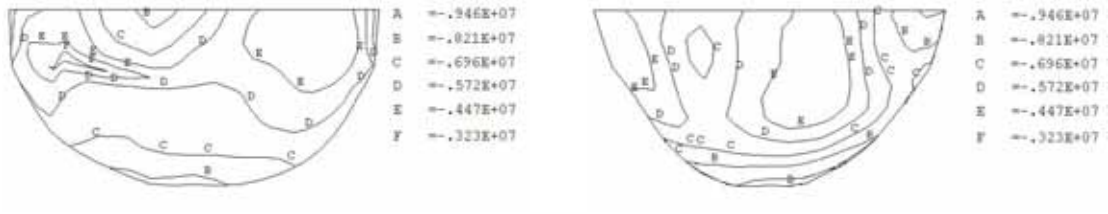

(a) upstream face (b) downstream face

Fig.3 Distribution of the third principle stress (model I, II and III), Mpa

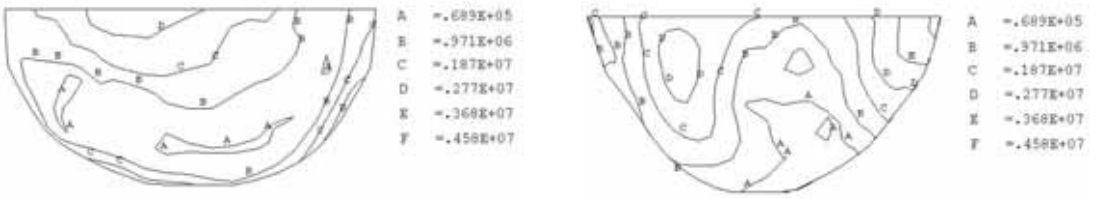

(a) upstream face (b) downstream face

Fig.4 Distribution of the first principle stress (model I), Mpa

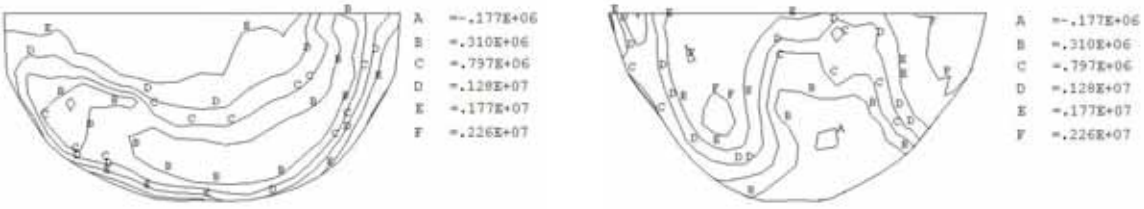

(a) upstream face (b) downstream face

Fig.5 Distribution of the first principle stress (model II), MPa

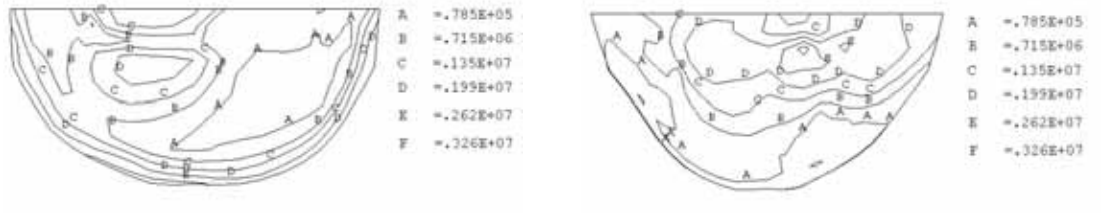

(a) upstream face (b) downstream face

Fig.6 Distribution of the first principle stress (model III), MPa

4.2. strain and strain rate of arch dam

The maximal equivalent strain of concrete in three cases were the same because the compressive strain of concrete played more important role on the equivalent strain of concrete in the dominant compressive stress states, although the tensile strain played more important role in the dominant tensile stress states but the values were smaller than the compressive strain. It was found that the maximal equivalent strain was 4.20×10^{-2} and it appeared at the bottom of the downstream face. Similarly, the maximal equivalent strain rates in three cases were the same and the maximal equivalent strain rate was up to $2.73\times10^{-2}s^{-1}$ and it also appeared at the bottom of the downstream face.

4.3. plastic strain and plastic strain rate of arch dam

The equivalent plastic strain of concrete appeared only on the tensile zones of arch dam. Fig.7 and fig.8 showed the distribution of the maximal equivalent plastic strain obtained from model II and model III, respectively. It was shown that the maximal equivalent plastic strain appeared on the bottom of the upstream face but it decreased 29.52% after taken account into the effect of strain rates. Fig.9 and fig.10 showed the distribution of the maximal equivalent plastic strain rates obtained from model II and model III, respectively. Similarly, the maximal equivalent plastic strain rate appeared on the bottom of the upstream face but it decreased 30.65% after taken account into the effect of strain rates.

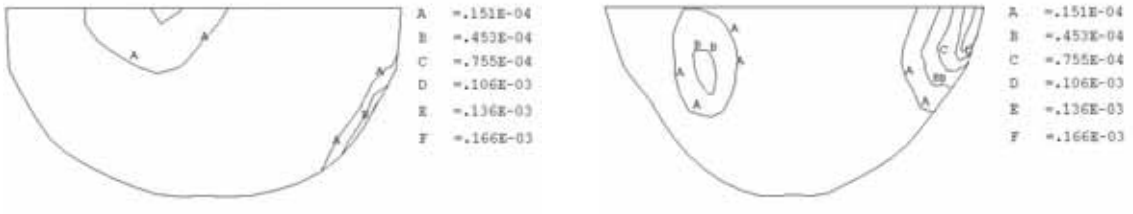

(a) upstream face (b) downstream face

Fig.7 Distribution of the equivalent viscoplastic strain (model II)

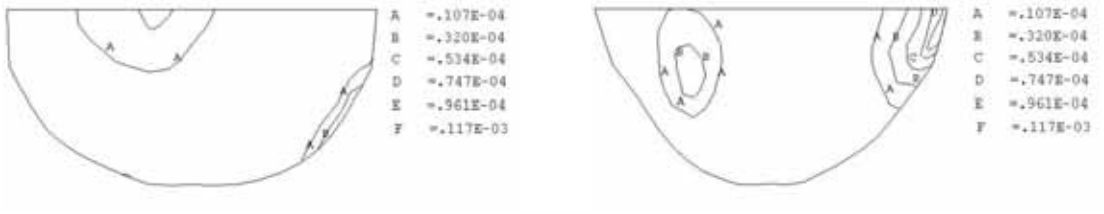

(a) upstream face (b) downstream face

Fig.8 Distribution of the equivalent viscoplastic strain (model III)

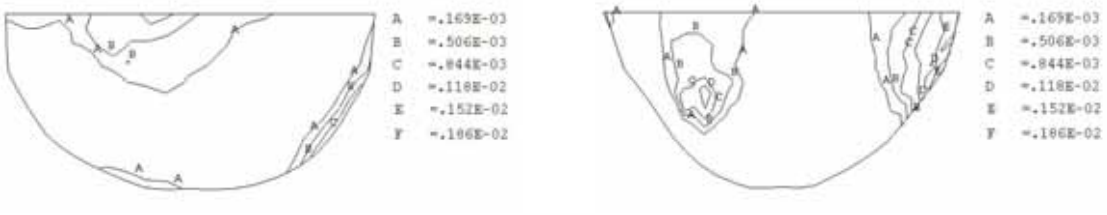

(a) upstream face (b) downstream face

Fig.9 Distribution of the equivalent viscoplastic strain rate (model II), s^{-1}

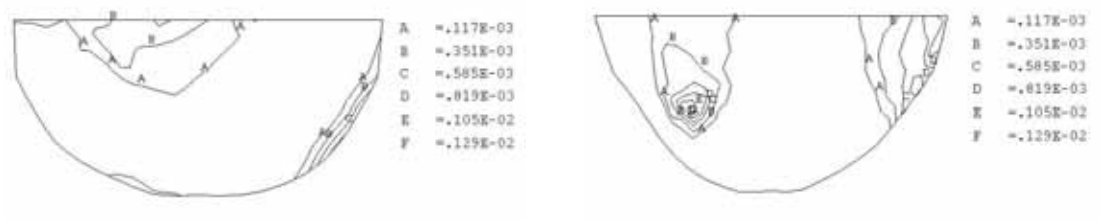

(a) upstream face (b) downstream face

Fig.10 Distribution of the equivalent viscoplastic strain rate (model III), s^{-1}

ACKNOWLEDGEMENTS

This study was founded by the National Science Foundation of China under grant No. 50408030 and the Innovation Group of Ministry of Education under grant No: IRT0518.

REFERENCES

Abrams, D.A. (1917). Effect of rate of Application of Load on the compressive strength of concrete. *ASTM J.* **17,** 364-377.

Bai, W.F., Chen, J.Y. and Zhong, H. (2006). Seismic overload response analysis of concrete gravity dam based on strain rate-dependent damage model. J*ournal of Hydraulic Engineering* **37:7,** 820-826. (Chinese)

Bischoff, P. H. and Perrry S.H. (1991). Compressive behaviour of concrete at high strain rates. *Materials and Structures* **24,** 425-450.

Cervera, M., Oliver, J. and Manzoli, O. (1996). A rate-dependent isotropic damage model for the seismic analysis of concrete dams. *Earthquake Engineering and Structural Dynamics* **25,** 987-1010.

Chen, J.Y., Hu, Z.Q. and Lin, G. (2004). Seismic analysis of arch dam with joints based on a new strain-rate-dependant plastic damage model. *Chinese Journal of Computational Mechanics* **21:1,** 45-49. (Chinese)

Chinese standard, (2001). Specifications for seismic design of hydraulic structures. Chinese Electric Power Press, Beijing.

Harris, D.W., Mohorovic, C.E. and Dolen, T.P. (2000). Dynamic properties of mass concrete obtained from dam cores. *ACI Material Journal* **97,** 290-296.

Lee, J. and Fenves, G.L. (1998). A plastic-damage concrete model for earthquake analysis of dams. *Earthquake Engineering and Structural Dynamics* **27,** 937-956.

Malvar, L.J. and Ross, C.A. (1998). Review of strain rate effects for concrete in tension. *ACI Materials Journal* **95:6,** 735-739.

Norris, G.H., Hansen, R.J., Holley, M.J., Biggs, J.M., Namyet, S. and Minami, J.K. (1959). Structural design for dynamic loads. McGraw-Hill Book Co., Inc., New York.

Raphael, J.M. (1984). Tensile strength of concrete. *ACI Journal* **87:17,** 158-165.

Rossi, P. and Toutlemonde, F. (1996). Effect of loading rate on the tensile behaviour of concrete: description of the physical mechanisms. *Materials and Structures* **29:186,** 116-118.

Rossi, P., Van, M. and Jan, G.M. (1994). Effect of loading rate on the strength of concrete subjected to uniaxial tension. *Materials and Structures* **27:169,** 260-264.

Tedesco, J.W., Ross, C.A., McGill, P.B. and O'Neil, B.P. (1991). Numerical Analysis of High Strain-Rate Concrete Direct Tension Tests. *Computers and Structures* **40:2,** 313-327.

Wang, W. (1997). Stationary and propagative instabilities in metals – a computational point of view. PhD, TU Delft, Netherlands.

Winnicke, A., Pearce, C.J. and Bicanic, N. (2001). Viscoplastic Hoffman consistency model for concrete. *Computers and structure* **79:1,** 7-19.

Xiao, S.Y., Li, H.N. and Lin, G. (2008). Dynamic behaviour and constitutive model of concrete at different strain rates. *Magazine of Concrete Research* **60:4,** 271-278

Zielinski, A.J., Reinhardt, H.W. and Körmeling, H.A. (1981). Experiments on concrete under uniaxial impact tensile loading. *Materials and Structures* **14:80,** 103-112.